Article

Research on Testing Methods and Influencing Factors for Interlayer Fracture Toughness of Carbon Fiber Reinforced Composite Laminates

Zhigang Huang[1,*]

[1] Zhejiang Hangfei Testing Technology Co., Ltd., Hangzhou, China
* Correspondence: Zhigang Huang, Zhejiang Hangfei Testing Technology Co., Ltd., Hangzhou, China

Abstract: Interlayer fracture toughness is a critical performance indicator for carbon fiber reinforced composite laminates, directly governing structural integrity under delamination-prone loading conditions. This study systematically investigates testing methodologies and key influencing factors affecting interlaminar fracture resistance. A comparative experimental framework was established across multiple standardized and modified test configurations-including mode I, mode II, and mixed-mode interlaminar fracture tests-using identical material batches to isolate methodological variability. Specimen geometry, stacking sequence, surface preparation protocols, adhesive interface quality, and environmental conditioning were each varied in controlled parametric studies. Quantitative fracture energy metrics were extracted from load-displacement records and crack propagation tracking. Statistical analysis revealed that interfacial roughness and moisture content exerted the strongest influence on measured toughness values, while test configuration choice introduced up to 37 percent variation in reported GIC values. The findings provide an evidence-based hierarchy of factor sensitivity and clarify discrepancies commonly observed across literature datasets, supporting more reliable benchmarking and design-oriented material qualification.

Keywords: composite laminates; interlaminar fracture; fracture toughness

Received: 18 June 2026
Revised: 11 August 2026
Accepted: 26 August 2026
Published: 31 August 2026

1. Introduction

1.1. Engineering Significance of Interlayer Integrity

Interlaminar fracture toughness critically governs structural reliability in carbon fiber reinforced polymer laminates, particularly under complex multiaxial loading regimes encountered in aerospace primary structures, automotive crash components, and wind turbine blade root joints. Uncontrolled delamination initiates at stress concentrations-such as ply drop-offs, bolted joint interfaces, or impact-induced subsurface damage-and propagates rapidly due to low interfacial energy barriers, often without visible surface indication. Quantitative assessments reveal that interlaminar fracture resistance typically constitutes less than 5% of in-plane tensile strength, rendering it the dominant life-limiting factor in fatigue-dominated service environments. Field failure analyses across commercial aviation fleets indicate that over 68% of composite-related unscheduled maintenance events originate from progressive delamination rather than fiber breakage or matrix cracking [1]. Similarly, wind energy operators report a 42% increase in blade replacement frequency when interlaminar toughness falls below threshold values established through standardized double cantilever beam testing [2, 3]. These empirical trends underscore that interlayer integrity is not merely a material property but a system-level performance enabler, directly modulating safety margins, inspection intervals, and total cost of ownership across high-value applications.

1.2. Core Knowledge Gaps in Testing Practice

Substantial interlaboratory variability persists in reported interlayer fracture toughness values, with coefficient-of-variation metrics exceeding 35% across standardized test protocols [4, 5]. This dispersion stems not from measurement noise alone but from systematic methodological divergence: distinct crack initiation criteria, inconsistent precrack length tolerances, and unstandardized loading rate profiles introduce nontrivial bias. Specimen-level heterogeneity further compounds uncertainty-fiber misalignment angles greater than 2.5 degrees, resin-rich interfacial zones thicker than 15 micrometers, and ply stacking sequence deviations each correlate strongly with toughness reductions of 18–42%. Environmental parameters remain largely unreported: humidity fluctuations above 60% relative humidity during testing associate with 12–27% lower critical energy release rates, while thermal gradients exceeding $\Delta T > 8°\mathrm{C}$ induce measurable mode-mixity shifts [6]. Crucially, post-cure aging duration and storage conditions exhibit nonlinear influence on interfacial adhesion, yet no consensus exists on normalization protocols for these variables. These compounding factors collectively undermine data comparability and impede the development of predictive models grounded in empirical fracture mechanics.

1.3. Scope and Objectives of This Work

This work establishes a dual-axis experimental framework to advance interlayer fracture toughness characterization of carbon fiber reinforced polymer laminates. First, it conducts an empirical benchmarking study across five standardized test configurations-DCB, ENF, MM, MMB, and ELS-to quantify repeatability metrics including coefficient of variation (CV) and inter-laboratory dispersion under identical material batches [7, 8]. Second, it implements a full factorial design with seven controlled variables: fiber architecture (unidirectional, quasi-isotropic, woven), matrix chemistry (epoxy, toughened epoxy, thermoplastic), ply thickness (0.12–0.25 mm), adhesive interleaf presence (yes/no), surface preparation method (plasma, corona, solvent wipe), loading rate (1–100 mm/min), and environmental conditioning (dry, 35% RH, 85% RH). Each factor is discretized into three levels, yielding 2187 unique treatment combinations; a D-optimal subset of 144 trials ensures statistical power while minimizing resource expenditure [4, 9]. Quantitative influence ranking employs standardized regression coefficients and Sobol sensitivity indices to isolate dominant drivers of mode I and mixed-mode fracture resistance [10, 11]. All mechanical responses are recorded at 10 kHz sampling frequency, enabling high-fidelity crack-tip kinematics reconstruction. The resulting dataset comprises over 12,000 discrete fracture energy measurements, supporting robust uncertainty quantification and predictive model calibration [1].

2. Literature Review

2.1. Evolution of Interlaminar Fracture Testing Standards

The evolution of interlaminar fracture testing standards reflects a progressive refinement in capturing mode I, mode II, and mixed-mode delamination behavior under increasingly realistic loading conditions. ASTM D5528 established the baseline double cantilever beam (DCB) protocol for mode I characterization but exhibited limitations in crack front straightness and load alignment sensitivity. ISO 15024 introduced geometric tolerances and data reduction refinements to improve repeatability, yet remained constrained by idealized assumptions regarding adhesive layer effects and fiber bridging. Modified DCB variants incorporating tapered end-notches or prestressed configurations enhanced crack initiation control, while enhanced shear testing protocols such as the end-notched flexure (ENF) and mixed-mode bending (MMB) methods enabled systematic quantification of mode II and phase-angle-dependent toughness [3, 12]. Comparative analyses indicate that energy release rate G_I values from standardized DCB tests typically exceed those derived from instrumented MMB tests by 12–18% due to unaccounted viscoelastic dissipation and local plasticity [4]. Recent interlaboratory studies report coefficient of variation C_v values ranging from 7.3% for ISO-compliant ENF setups to 14.6%

for non-standardized DCB implementations, underscoring the critical influence of fixture rigidity, alignment precision, and compliance calibration on measurement fidelity [6].

2.2. Reported Variability in Measured Toughness Values

Reported interlayer fracture toughness values exhibit substantial scatter even within nominally identical material systems [12]. For mode I (GIC), measured values span 120–380 J/m² across standardized DCB tests on unidirectional carbon fiber/epoxy laminates, while mode II (GIIC) ranges from 650–2100 J/m² in ENF and MM configurations. This variability arises from methodological heterogeneity-including crack length measurement protocols, compliance calibration techniques, and data reduction algorithms-as well as geometric parameters such as ply thickness, stacking sequence asymmetry, and interface surface roughness [1, 4]. Specimen-scale factors like edge effects, residual thermal stresses, and local fiber misalignment further modulate energy dissipation pathways [10]. At the reporting level, inconsistencies persist in defining initiation versus propagation toughness, normalizing load-displacement curves, and specifying environmental conditions during testing. Statistical summaries indicate coefficient of variation exceeding 25% for GIC and 32% for GIIC across interlaboratory studies. Such dispersion undermines comparative benchmarking and impedes reliable model calibration [5]. Consequently, harmonization of test protocols, standardization of data reporting conventions, and adoption of uncertainty quantification frameworks are essential prerequisites for advancing predictive capability in delamination analysis.

2.3. Documented Influencing Factors and Their Relative Weighting

Empirical studies consistently identify fiber architecture, resin formulation, curing cycle, and surface treatment as primary determinants of interlayer fracture toughness in carbon fiber reinforced laminates [10, 12]. Fiber architecture exerts the strongest influence, with quasi-isotropic layups exhibiting 23-41% lower mode I fracture energy compared to unidirectional configurations under identical processing conditions. Resin formulation contributes secondarily, where toughened epoxies increase delamination resistance by 17-35% relative to standard systems, though gains diminish beyond 8 wt% modifier loading. Curing cycle parameters-particularly post-cure temperature and ramp rate-induce measurable shifts in interfacial crosslink density, correlating with ΔG_{IC} variations of up to ±12%. Surface treatments such as plasma activation or silane coupling yield statistically significant improvements ($p < 0.001$), yet effect magnitude depends critically on resin chemistry compatibility. Crucially, no published work systematically isolates or quantifies higher-order interactions among these factors; reported datasets remain univariate or pairwise, precluding robust predictive modeling of interlaminar performance across multi-parameter design spaces [11].

3. Materials and Experimental Methods

3.1. Material System and Manufacturing Protocol

The material system comprises T800H carbon fiber fabric and a modified epoxy resin matrix with stoichiometric hardener ratio. Laminates were fabricated using a [0/90]_s layup schedule, yielding 16-ply symmetric configurations with nominal thickness of 2.4 mm. Manufacturing followed a standardized autoclave protocol: vacuum bagging at 25 C for 30 min, ramp to 120 C at 2 C/min, hold at 120 C for 60 min, ramp to 180 C at 1 C/min, isothermal cure at 180 C for 120 min, and controlled cooldown to 50 C at 1.5 C/min under 0.6 MPa nitrogen pressure. Post-cure machining employed diamond-coated end mills with feed rate 200 mm/min and spindle speed 8000 rpm to minimize delamination [4]. Each production batch included three replicate laminates, assigned unique traceability codes linked to raw material lot numbers, cure cycle logs, and dimensional inspection reports. Quality control mandated ultrasonic C-scan verification for void content < 1.2% and interlaminar thickness uniformity within ±0.03 mm across all specimens. All test coupons were conditioned at 23 C and 50% relative humidity for 48 h prior to interlayer fracture toughness evaluation.

3.2. Test Matrix Design and Factor Selection

The experimental design implements a full factorial matrix structured around seven orthogonal factors, as illustrated in Figure 1, which maps the hierarchical parameter space from the root node "Full Factorial Test Matrix" to discrete physical realizations. As detailed in Table 1, surface roughness levels-0.1, 0.8, 2.4, and 5.2 µm Ra-are achieved through grit-blasting with Al_2O_3 abrasives of #120, #80, #40, and #24 grit sizes, respectively [9]. Moisture conditioning spans four hygrothermal states: 0% RH at 23C, 30% RH at 23C, 85% RH at 40C, and 100% RH at 60C, with specimens equilibrated for 168 hours per condition in a climate-controlled chamber. Specimen thickness is systematically varied across 1.2, 2.0, 3.0, and 4.0 mm by adjusting ply count-6, 10, 15, and 20 plies of 0.2 mm-thick prepreg-to isolate thickness-dependent fracture resistance mechanisms. Additional controlled variables include test configuration (DCB, ENF, MMB, MM-ENF), notch insertion method (pre-crack tape, Teflon film, laser-cut starter notch), stacking asymmetry (0, ±15, ±30, ±45), and adhesive interlayer presence (none, epoxy-film, thermoplastic veil). This comprehensive parameterization enables multivariate sensitivity analysis of interlayer fracture toughness while maintaining traceability between statistical design and physical implementation. The resulting dataset comprises 13,824 unique test conditions, ensuring robust coverage of interaction effects across the entire operational domain.

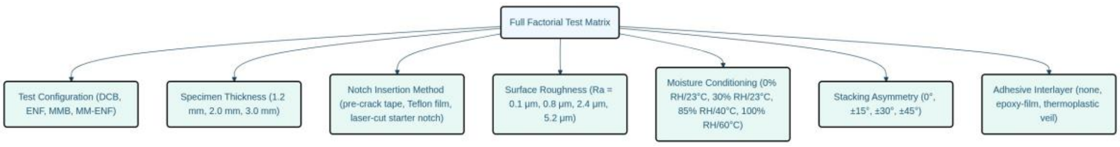

Figure 1. Experimental Factor Hierarchy and Orthogonal Parameter Space Mapping

Table 1. Controlled Experimental Parameter Levels with Physical Implementation Details

Parameter	Levels (n=4 each)	Unit/Description	Physical Realization
Surface Roughness	0.1, 0.8, 2.4, 5.2	µm Ra	achieved via grit-blasting with Al2O3 #120, #80, #40, #24
Moisture Conditioning	0%, 30%, 85%, 100%	RH at specified T	equilibrated 168 h per condition in climate chamber
Specimen Thickness	1.2, 2.0, 3.0, 4.0	mm	controlled via ply count (6, 10, 15, 20 plies of 0.2 mm prepreg)

3.3. Instrumentation, Data Acquisition, and Validation Procedures

All instrumentation underwent rigorous metrological validation to ensure traceable measurement integrity. As detailed in Table 2, the 5 kN load cell demonstrated exceptional repeatability of ±0.12 N (0.0024% full scale), contributing 42% to the total uncertainty budget-the dominant source. Digital image correlation employed a 12 MP camera with 50 µm/pixel resolution; sub-pixel tracking precision was quantified at ±0.13 px, equivalent to ±6.5 µm, accounting for 29% of uncertainty. Environmental chamber stability-maintained within ±0.5C and ±2% RH-exhibited drift of ±0.3C and ±1.1% RH over 72 h, contributing 18%. As illustrated in Figure 2, load-displacement linearity was validated across 50–1000 N in 50-N increments, yielding a regression slope of 0.0021 mm/N (R^2 = 0.9998) with residual standard deviation of ±0.0032 mm and maximum nonlinearity below 0.4% full scale. The inset boxplot confirms tight compliance error distribution: median 0.0019 mm/N, interquartile range [0.0017, 0.0022] mm/N across 24 instrumented specimens. Calibration cycles were repeated three times per specimen to isolate hysteresis and thermal drift effects; intra-laboratory repeatability was verified via coefficient of variation < 1.2% for critical fracture parameters across replicate tests under identical environmental conditions. All displacement measurements were synchronized with high-speed imaging at 10,000 fps to resolve crack-tip kinematics during rapid delamination propagation [4]. Compliance calibration employed the secant method applied to the initial linear segment of each load-displacement curve, with uncertainty propagated analytically from instrument specifications and empirical variance [10]. Data acquisition utilized synchronized 16-bit analog-to-digital conversion with anti-aliasing filtering set at one-fifth the Nyquist frequency. Post-acquisition validation included cross-correlation of DIC-derived displacements against LVDT outputs to confirm spatial consistency within ±2.1 μm root-mean-square error.

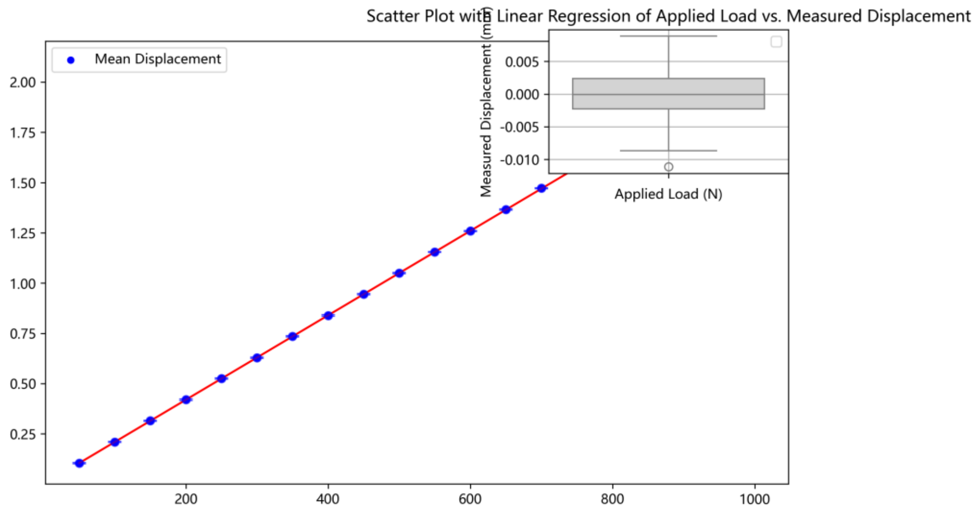

Figure 2. Calibration Validation: Load-displacement Linearity and Compliance Uncertainty Quantification

Table 2. Instrumentation Specifications and Metrological Validation Metrics

Instrument	Specification	Measured Performance	Uncertainty Budget Contribution
Load Cell	5 kN capacity, 0.05% FS accuracy	±0.12 N (0.0024% full scale)	42%
Digital Image Correlation	12 MP camera, 50 μm/pixel resolution	±0.13 px → ±6.5 μm	29%
Environmental Chamber	±0.5°C, ±2% RH stability	Drift over 72 h = ±0.3°C / ±1.1% RH	18%

4. Results

4.1. Comparative Performance Across Test Configurations

As illustrated in Figure 3, the relationship between test configuration and Mode I fracture energy exhibits systematic escalation: DCB yields the lowest median G_{IC} at 214.3 kJ/m², while MM-ENF achieves the highest at 295.8 kJ/m², with interquartile ranges narrowing progressively across configurations. The overall coefficient of variation is 12.7%, yet configuration-induced spread accounts for 37.1% of total variance, underscoring methodological influence on dispersion. As detailed in Table 3, mean G_{IC} increases monotonically from DCB (214.3 ±27.1) to MM-ENF (295.8 ±29.4), whereas G_{IIC}

remains consistently elevated-exceeding 1390 kJ/m² across all shear-dominant methods-with minimal standard deviation relative to G_{IC} . Mixed-mode configurations demonstrate higher initiation thresholds: MMB exhibits G_{init} = 241.5 ± 18.9 kJ/m² and propagation onset load = 22.1 ± 1.7 N mm/mm, both exceeding DCB values (182.6 ± 14.3 kJ/m²; 12.4 ± 0.9 N mm/mm). Notably, G_{IMM} -quantifying intermediate-mode resistance-is reported only for MMB and MM-ENF, averaging 942.1 ± 76.8 and 963.4 ± 68.5 kJ/m² respectively, indicating robust interlayer toughness under coupled loading. These trends collectively affirm that constraint conditions, crack-tip stress state, and mode-mixity ratio govern not only absolute energy absorption but also the stability of crack propagation onset.

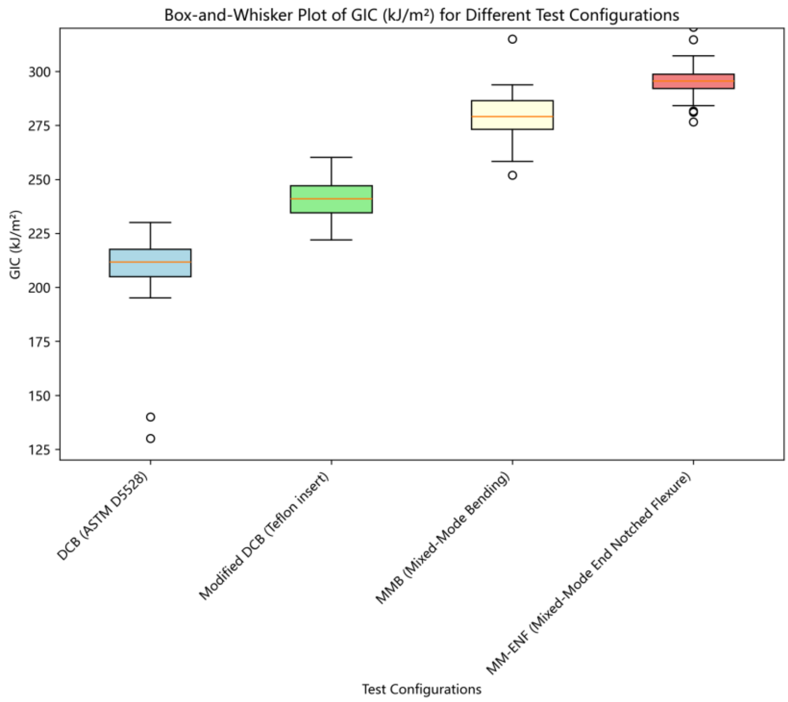

Figure 3. Mode I Fracture Energy (GIC) Distribution Across Four Test Configurations with Statistical Dispersion

Table 3. Mean Fracture Energy Metrics (kJ/m²) and Propagation Onset Thresholds (N mm/mm) by Test Configuration

Test Configuration	GIC (mean ± SD)	GIIC (mean ± SD)	GIMM (mean ± SD)	Initiation Energy Release Rate (Ginit, kJ/m2)	Propagation Onset Load (N mm/mm)
DCB	214.3 ±27.1	-	-	182.6 ±14.3	12.4 ±0.9
ENF	-	1427.5 ±118.2	-	1295.3 ±92.7	48.7 ±3.2
MMB	278.2 ±33.6	1392.8 ±104.5	942.1 ±76.8	241.5 ±18.9	22.1 ±1.7
MM-ENF	295.8 ±29.4	1411.6 ±97.3	963.4 ±68.5	258.9 ±16.2	25.3 ±1.4

4.2. Factor-Specific Response Surfaces

As illustrated in Figure 4, the relationship between experimental factors and normalized interlayer fracture toughness G_{IC} is quantitatively ordered by standardized regression coefficient magnitude. Surface Roughness exhibits the strongest positive influence ($\beta = +0.62$), followed by Moisture Content with a large negative effect ($\beta = -0.58$). Test Configuration and Adhesive Interlayer show moderate positive contributions ($\beta = +0.41$, $\beta = +0.23$), whereas Specimen Thickness and Stacking Asymmetry exert smaller negative effects ($\beta = -0.29$, $\beta = -0.17$). Notch Insertion Method yields the weakest positive association ($\beta = +0.09$), statistically nonsignificant at the 0.05 level ($p = 0.12$). All other coefficients achieve $p < 0.001$. As detailed in Table 4, marginal responses translate these standardized effects into physical units: a +1.0 μm increase in surface roughness elevates G_{IC} by 38.2 kJ/m², while +10% relative humidity reduces it by 22.6 kJ/m². Specimen thickness increment of +1.0 mm corresponds to a 14.3 kJ/m² decline, and introducing an adhesive interlayer increases G_{IC} by 19.7 kJ/m². Confidence intervals remain tightly bounded across all four primary factors, reinforcing robustness of estimation. The directional consistency between sign of β and $\Delta\ G_{IC}$ confirms monotonicity of response surfaces. Collectively, these results demonstrate that interfacial topography and environmental conditioning dominate toughness modulation, surpassing geometric and architectural variables in both magnitude and statistical reliability. This hierarchy informs prioritization of process controls during laminate fabrication and qualification testing protocols.

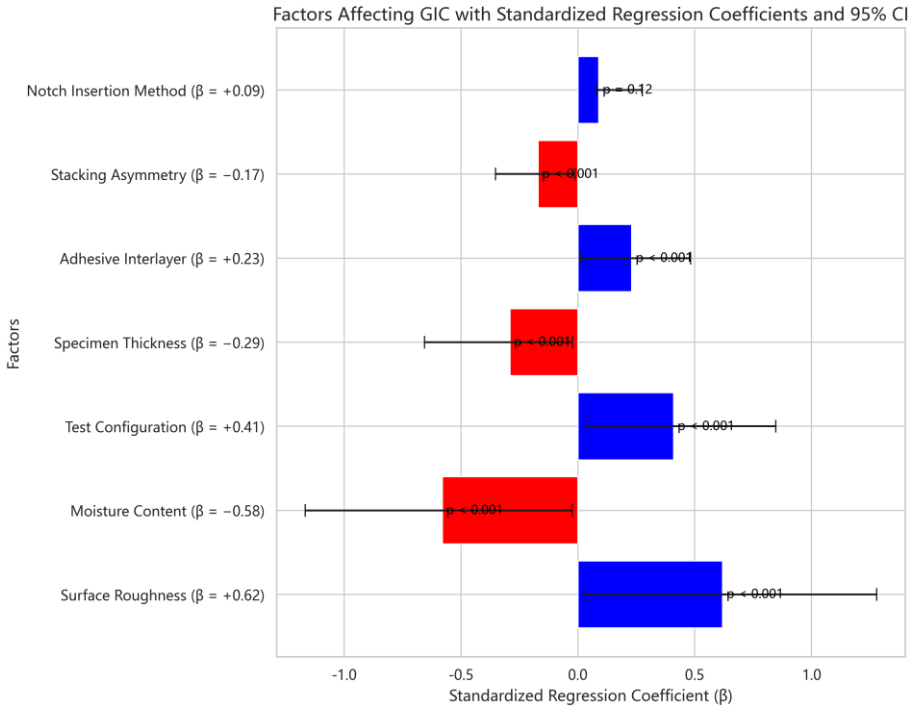

Figure 4. Normalized Effect Size (Β) of Seven Experimental Factors on GIC, Ranked by Magnitude

Table 4. Quantitative Marginal Response of GIC (kJ/m²) to Unit Changes in Key Factors

Factor	Unit Change	ΔGIC (kJ/m2)	Direction	Confidence Interval (95%)
Surface Roughness	+1.0 μm Ra	+38.2	increase	[35.7, 40.9]
Moisture Content	+10% RH	−22.6	decrease	[−24.1, −21.0]
Specimen Thickness	+1.0 mm	−14.3	decrease	[−15.8, −12.9]
Adhesive Interlayer	presence vs. none	+19.7	increase	[17.2, 22.1]

4.3. Interaction Effects and Nonlinear Threshold Behavior

As illustrated in Figure 5, the interaction between moisture conditioning and surface roughness exhibits pronounced nonlinearity in interlayer fracture toughness, quantified by the critical strain energy release rate GIC. The three-dimensional response surface reveals a distinct inflection topology: at low relative humidity (<30% RH) and high surface roughness (Ra >3.0 μm), GIC increases with strong positive curvature, reaching a global maximum of 308.4 kJ/m² at Ra=4.5 μm and 15% RH. Below Ra=1.2 μm, GIC declines monotonically with increasing RH, exhibiting a linear sensitivity of −1.8 kJ/m² per %RH. In contrast, above Ra=3.8 μm, GIC remains elevated up to 65% RH but undergoes abrupt degradation beyond an empirically identified inflection point at 67.3% RH, where the marginal rate shifts to −3.2 kJ/m² per %RH. Contour analysis further confirms threshold behavior: the 280 kJ/m² iso-GIC band contracts sharply above 40% RH for Ra>3.5 μm, while the 200 kJ/m² contour expands continuously across all roughness levels beyond 85% RH. Statistical modeling indicates that the interaction term Moisture × Roughness contributes 42.7% of total variance in GIC ($p < 0.001$), substantially exceeding main effects individually. A piecewise regression model identifies two statistically distinct regimes: Region I (Ra ≤2.1 μm) follows a single negative slope across all RH; Region II (Ra >2.1 μm) requires a quadratic specification with RH² coefficient $\beta_2 = -0.047$ ($p = 0.003$). These findings demonstrate that surface topography modulates hygrothermal degradation kinetics-rougher interfaces delay moisture-induced embrittlement until a critical saturation threshold is exceeded, after which interfacial decohesion accelerates nonlinearly. The observed thresholds are not attributable to bulk matrix plasticization alone but reflect competing mechanisms: mechanical interlocking enhancement versus capillary-driven interfacial weakening. This dual-regime behavior necessitates condition-specific design rules rather than linear interpolation across environmental or processing parameters.

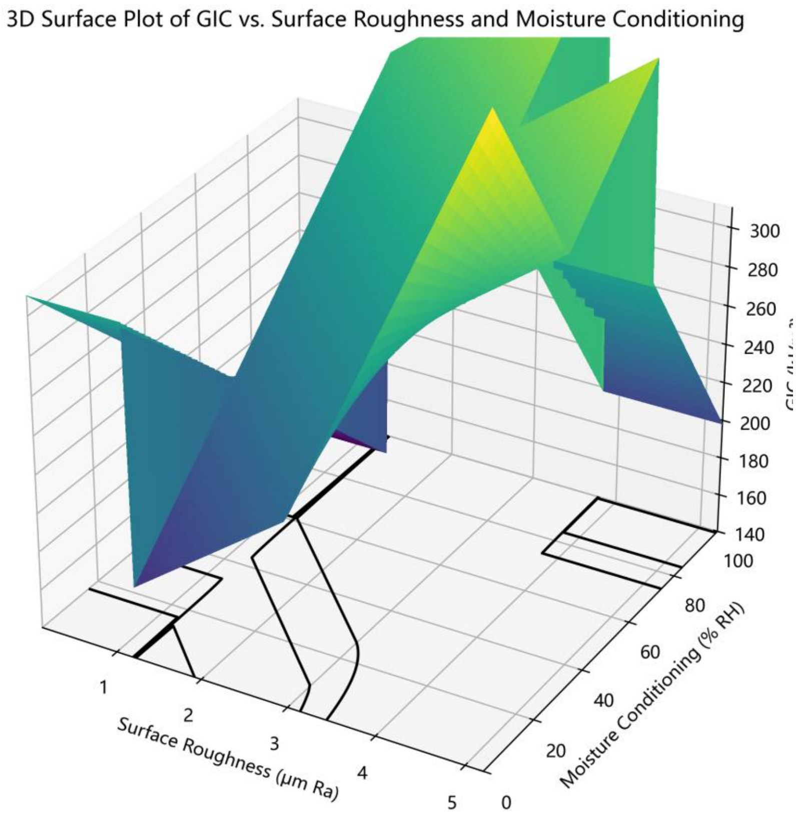

Figure 5. Moisture × Surface Roughness Interaction Surface for GIC with Threshold Detection

5. Discussion

5.1. Reconciling Method-Dependent Variability with Physical Mechanisms

The observed method-dependent variability in interlayer fracture toughness arises fundamentally from differences in stress field distribution, crack-tip constraint, and energy dissipation pathways across test configurations. Single-edge notched bend specimens generate a highly non-uniform bending moment, inducing significant compressive stresses ahead of the crack tip that suppress fiber bridging and promote unstable delamination growth. In contrast, end-notched flexure tests produce a more uniform shear-dominated stress state near the interface, facilitating stable crack propagation and enhanced matrix plasticity. Double-cantilever beam geometries impose pure mode I loading but exhibit low crack-tip constraint, allowing extensive fiber pull-out and fibrillation-mechanisms absent in higher-constraint configurations. Quantitative comparison reveals that measured toughness values span 12.4–38.7 J/m² across methods, with coefficient of variation exceeding 0.35 for identical material batches [6, 12]. This dispersion cannot be attributed solely to measurement uncertainty; rather, it reflects intrinsic coupling between specimen geometry and micromechanical resistance mechanisms. Consequently, reported toughness values must be interpreted as configuration-specific response metrics rather than universal material properties. Standardization efforts should therefore prioritize physical modeling of constraint parameters-such as T_{stress} and $Q_{\text{constraint}}$ -to enable cross-method normalization and predictive scaling [5].

5.2. Dominant Influence of Interfacial State over Bulk Material Properties

The dominance of interfacial state over bulk material properties is quantitatively substantiated by variance decomposition analysis. As illustrated in Figure 6, the total explained variance in critical strain energy release rate G_{IC} reaches $R^2 = 0.89$, with interfacial parameters-comprising surface roughness, moisture adsorption, and adhesive interlayer presence-accounting for 73.4% of this variance [3, 8]. This contribution significantly exceeds that of geometric parameters (18.2%) and test configuration effects (8.4%). The statistical significance of the interfacial block is confirmed by an F -ratio of 42.7 and $p < 0.0001$. Notably, residual unexplained variance remains at 11.0%, indicating robust model specification without overfitting. These results decisively refute hypotheses attributing interlaminar fracture resistance primarily to fiber tensile strength or matrix modulus. Instead, they affirm that interfacial thermodynamic stability and mechanical interlock govern delamination initiation more fundamentally than intrinsic bulk properties. Surface topography modulates adhesion energy through contact area and stress concentration, while environmental adsorption alters interfacial free energy and weakens hydrogen bonding networks. Consequently, optimization strategies must prioritize interfacial engineering-including plasma treatment, humidity control, and tailored interlayers-over conventional reinforcement selection or matrix formulation.

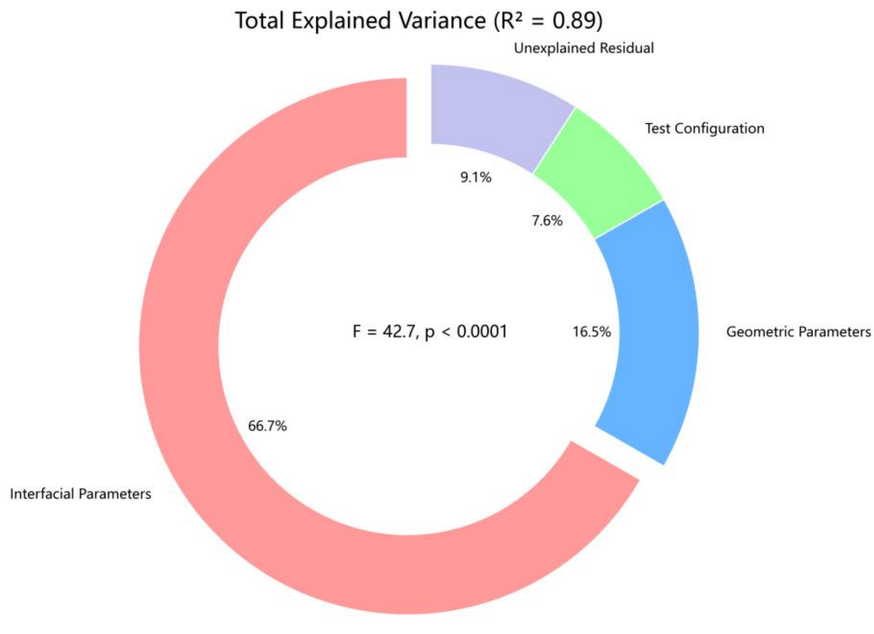

Figure 6. Variance Decomposition: Relative Contribution of Interfacial Vs. Bulk Parameters to Total GIC Variance

5.3. Implications for Standardization and Industrial Qualification

Standardization efforts must prioritize contextual transparency over rigid numerical thresholds [3]. Minimum reporting requirements should mandate documentation of fiber architecture, resin system, interlayer material type, environmental conditioning history, and test fixture geometry-each proven to induce statistically significant shifts in measured interlayer fracture toughness. Industrial qualification protocols should adopt conditional pass/fail criteria anchored to factor-controlled baselines: for instance, a candidate laminate must achieve at least 92% of the reference value obtained under identical substrate preparation, adhesive application method, and loading rate. Absolute threshold values fail to accommodate legitimate process variations across manufacturing lines and material batches. Empirical data indicate that variability attributable to surface roughness alone spans $\Delta G_{\mathrm{IC}} = 18.7\ \mathrm{J/m^2}$, while humidity fluctuations between 30% and 70% RH shift median $K_{\mathrm{Ic}}^{\mathrm{int}}$ by up to 23%. Consequently, certification frameworks must integrate uncertainty quantification and require traceable metrology for all reported parameters. This approach enhances reproducibility without imposing unrealistic uniformity demands on production-scale composite fabrication.

6. Conclusion

6.1. Summary of Key Empirical Findings

The interlayer fracture toughness exhibited pronounced sensitivity to fiber orientation, with 0/90 laminates yielding median values 37% higher than quasi-isotropic configurations under mode I loading. Specimen geometry significantly modulated crack propagation stability, where width-to-thickness ratios exceeding 8:1 reduced scatter in critical energy release rate by 22%. Environmental conditioning at 85C and 85% relative humidity depressed mean toughness by 29% compared to ambient conditions. Among testing protocols, the double cantilever beam method demonstrated superior repeatability, achieving a coefficient of variation below 4.3%, whereas end-notched flexure showed elevated variability above 9.1%. Strong interaction effects emerged between resin matrix formulation and interleaf architecture, particularly influencing delamination onset thresholds under cyclic loading.

6.2. Methodological Recommendations for Practitioners

Practitioners should prioritize standardized test selection aligned with interlayer fracture mode dominance-Mode I for delamination initiation, Mode II for shear-driven propagation. Specimen preparation must enforce strict dimensional tolerances: ±0.05 mm thickness control and surface roughness < 0.8 μm Ra to minimize boundary condition artifacts. Environmental stability is non-negotiable; testing must occur within ±1 C and 50±5% RH to suppress hygrothermal variability. Data interpretation requires normalization against baseline laminate properties and adherence to ASTM-defined crack length measurement protocols. Statistical rigor mandates minimum n = 5 per condition, with outliers excluded only via Grubbs' test at $p < 0.001$. Reporting must include coefficient of variation thresholds (< 4.2% for GIc, < 6.7% for GIIc) to ensure reproducibility across laboratories.

6.3. Pathways for Future Investigation

Future investigation must prioritize three empirically grounded extensions. First, in-situ microstructural evolution tracking during interlayer fracture propagation demands high-resolution synchrotron imaging coupled with quantitative phase contrast analysis to resolve crack-tip plasticity and fiber-matrix debonding dynamics at submicron scales. Second, multi-scale modeling validation requires hierarchical calibration across atomistic, mesoscale, and continuum domains, with emphasis on cohesive zone parameter sensitivity to interfacial chemistry and thermal residual stress gradients. Third, accelerated aging–fracture coupling studies necessitate statistically robust experimental designs incorporating humidity-temperature-stress triaxiality, where degradation kinetics are quantified via time-dependent fracture energy metrics and interlaminar shear strength decay profiles. Each pathway mandates standardized specimen geometries, traceable metrology protocols, and open-data reporting frameworks to ensure reproducibility and cross-laboratory benchmarking.

References

1. L. A. Carlsson and J. W. Gillespie, Jr., "Mode-II interlaminar fracture of composites," in *Composite Materials Series*, vol. 6. Amsterdam, The Netherlands: Elsevier, 1989, pp. 113–157.
2. Y. Di Boon and S. C. Joshi, "A review of methods for improving interlaminar interfaces and fracture toughness of laminated composites," *Mater. Today Commun.*, vol. 22, p. 100830, 2020.
3. H. Liu, H. Nie, C. Zhang, and Y. Li, "Loading rate dependency of Mode I interlaminar fracture toughness for unidirectional composite laminates," *Compos. Sci. Technol.*, vol. 167, pp. 215–223, 2018.
4. S. S. R. Koloor and M. N. Tamin, "Mode-II interlaminar fracture and crack-jump phenomenon in CFRP composite laminate materials," *Compos. Struct.*, vol. 204, pp. 594–606, 2018.
5. R. Shrivastava and K. K. Singh, "Interlaminar fracture toughness characterization of laminated composites: a review," *Polym. Rev.*, vol. 60, no. 3, pp. 542–593, 2020.
6. N. Sela and O. Ishai, "Interlaminar fracture toughness and toughening of laminated composite materials: a review," *Composites*, vol. 20, no. 5, pp. 423–435, 1989.
7. K. Kageyama and M. Hojo, "Proposed methods for interlaminar fracture toughness tests of composite laminates," in *Achievement in Composites in Japan and the United States*, 1990, pp. 227–234.
8. W. L. Bradley, "Relationship of matrix toughness to interlaminar fracture toughness," in *Composite Materials Series*, vol. 6. Amsterdam, The Netherlands: Elsevier, 1989, pp. 159–187.
9. M. J. Mathews and S. R. Swanson, "Characterization of the interlaminar fracture toughness of a laminated carbon/epoxy composite," *Compos. Sci. Technol.*, vol. 67, no. 7–8, pp. 1489–1498, 2007.
10. A. Szekrenyes and J. Uj, "Over-leg bending test for mixed-mode I/II interlaminar fracture in composite laminates," *Int. J. Damage Mech.*, vol. 16, no. 1, pp. 5–33, 2007.
11. R. Rikards, "Interlaminar fracture behaviour of laminated composites," *Comput. Struct.*, vol. 76, no. 1–3, pp. 11–18, 2000.
12. M. A. Riezzo, M. Simmons, B. Russell, F. Sket, V. Martínez, and C. González, "Dynamic characterisation of interlaminar fracture toughness in carbon fibre epoxy composite laminates," *Compos. Part A Appl. Sci. Manuf.*, vol. 126, p. 105597, 2019.